Structural Basis for Iron Mineralization by Bacterioferritin

Allister Crow,[†] Tamara L. Lawson,[‡] Allison Lewin, Geoffrey R. Moore, and
Nick E. Le Brun*

*Centre for Molecular and Structural Biochemistry, School of Chemical Sciences and Pharmacy,
University of East Anglia, Norwich NR4 7TJ, U.K.*

Received November 30, 2008; E-mail: n.le-brun@uea.ac.uk

Abstract: Ferritin proteins function to detoxify, solubilize and store cellular iron by directing the synthesis of a ferric oxyhydroxide mineral solubilized within the protein's central cavity. Here, through the application of X-ray crystallographic and kinetic methods, we report significant new insight into the mechanism of mineralization in a bacterioferritin (BFR). The structures of nonheme iron-free and di-Fe^{2+} forms of BFR showed that the intrasubunit catalytic center, known as the ferroxidase center, is preformed, ready to accept Fe^{2+} ions with little or no reorganization. Oxidation of the di-Fe^{2+} center resulted in a di-Fe^{3+} center, with bridging electron density consistent with a μ-oxo or hydro bridged species. The μ-oxo bridged di-Fe^{3+} center appears to be stable, and there is no evidence that Fe^{3+} species are transferred into the core from the ferroxidase center. Most significantly, the data also revealed a novel Fe^{2+} binding site on the inner surface of the protein, lying ~10 Å directly below the ferroxidase center, coordinated by only two residues, His46 and Asp50. Kinetic studies of variants containing substitutions of these residues showed that the site is functionally important. In combination, the data support a model in which the ferroxidase center functions as a true catalytic cofactor, rather than as a pore for the transfer of iron into the central cavity, as found for eukaryotic ferritins. The inner surface iron site appears to be important for the transfer of electrons, derived from Fe^{2+} oxidation in the cavity, to the ferroxidase center. Bacterioferritin may represent an evolutionary link between ferritins and class II di-iron proteins not involved in iron metabolism.

Introduction

The ability to store iron in a bioavailable and safe form is a central feature of the strategy Nature has evolved to overcome the dual problem of poor bioavailability of iron and the potential of the free metal to catalyze the formation of extremely reactive radical species.[1] The function of iron storage is fulfilled by the ferritin family of proteins, in which subunits are arranged in a highly symmetric fashion to form an approximately spherical protein coat surrounding a hollow center. Large amounts of iron can be stored within the central cavity, in the form of a ferric-oxy-hydroxide mineral core.[2,3]

Mineralization occurs when iron, as Fe^{2+}, is taken up by the protein, oxidized to Fe^{3+}, and hydrated. In 24-meric ferritins, a dinuclear metal ion binding site, known as the ferroxidase center, which is found within H-chain-type subunits (but not in L-chains, the other major subunit type), is key to this activity.[4] In eukaryotic H-chain ferritins the ferroxidase center has been

shown to function as a gated site for the transfer of Fe^{3+} into the cavity following oxidation[5,6] and is required for core nucleation.[6]

Bacterioferritins (BFRs), which are unique among ferritins in that they contain up to 12 *b*-type heme groups,[7] are composed of 24 H-chain-like subunits. However, the BFR ferroxidase center is distinct from those of other H-chain subunits, bearing a much closer relationship to the centers of class II di-iron proteins such as ribonucleotide reductase and soluble methane monooxygenase.[7,8] These structural differences result in distinct mechanistic and functional properties. For example, spectroscopic and kinetic studies showed that the oxidized form of the ferroxidase center of *Escherichia coli* BFR is stable and is required throughout core formation.[9-11]

To gain further insight into the mechanism of mineralization in BFR, we have applied a combination of X-ray crystallography and kinetic methods. We report the high resolution structural

[†] Current address: Department of Biological Chemistry, John Innes Centre, Norwich Research Park, Colney, Norwich NR4 7UH, UK.

[‡] Current address: Department of Biochemistry and Molecular Biology, University of British Columbia, Life Sciences Centre, 2350 Health Sciences Mall, Vancouver, BC V6T 1Z3 Canada.

(1) Lewin, A.; Moore, G. R.; Le Brun, N. E. *Dalton Trans.* **2005**, 3597–3610.

(2) Andrews, S. C. *Iron storage in bacteria*; Academic Press: 1998; Vol. 40, pp 281–351.

(3) Theil, E. C. *Adv. Enzymol. Relat. Areas Mol. Biol.* **1990**, *63*, 421–449.

(4) Chasteen, N. D. *Metal Ions Biol. Sys.* Vol. 35, **1998**, *35*, 479–514.

(5) Bou-Abdallah, F.; Zhao, G. H.; Mayne, H. R.; Arosio, P.; Chasteen, N. D. *J. Am. Chem. Soc.* **2005**, *127*, 3885–3893.

(6) Zhao, G. H.; Bou-Abdallah, F.; Arosio, P.; Levi, S.; Janus-Chandler, C.; Chasteen, N. D. *Biochemistry* **2003**, *42*, 3142–3150.

(7) Frolow, F.; Kalb, A. J.; Yariv, J. *Nat. Struct. Biol.* **1994**, *1*, 453–460.

(8) Le Brun, N. E.; Andrews, S. C.; Guest, J. R.; Harrison, P. M.; Moore, G. R.; Thomson, A. J. *Biochem. J.* **1995**, *312*, 385–392.

(9) Le Brun, N. E.; Wilson, M. T.; Andrews, S. C.; Guest, J. R.; Harrison, P. M.; Thomson, A. J.; Moore, G. R. *FEBS Lett.* **1993**, *333*, 197–202.

(10) Yang, X.; Le Brun, N. E.; Thomson, A. J.; Moore, C. R.; Chasteen, N. D. *Biochemistry* **2000**, *39*, 4915–4923.

(11) Baaghil, S.; Lewin, A.; Moore, G. R.; Le Brun, N. E. *Biochemistry* **2003**, *42*, 14047–14056.

characterization of nonheme iron free, di-Fe^{2+}, and μ-oxo bridged di-Fe^{3+} forms of the catalytic ferroxidase center and a novel iron site located on the inner surface of the protein, relatively close to the ferroxidase center, in which the iron is ligated by only two residues, His46 and Asp50. Site-directed variants of BFR lacking one or both of these residues are significantly disrupted in their capacity to form an iron core but are essentially unaffected in terms of their ferroxidase center activities. A model is discussed in which both the inner surface iron site and the ferroxidase center are essential for mineralization.

Experimental Section

Strains, Growth Media, and Site-Directed Mutagenesis. *Escherichia coli* strains JM109 and AL1 (BL21(DE3) *bfr⁻*)[11] were used for site-directed mutagenesis and expression, respectively, and grown at 37 °C in LB (Luria−Bertani) broth, on LA plates consisting of LB broth with 1.25% (w/v) agar. Ampicillin, where appropriate, was used at a concentration of 100 mg/L. Site directed mutants encoding H46A and D50A BFR were generated using a whole-plasmid method, employing pALN1 (a pET21a derivative containing wild-type *bfr*, generated by ligating the *Nde*I and *Eco*RI fragment from pGS758[10] into pET21a (Novagen) cut with the same enzymes) as a template. Resulting plasmids encoding H46A BFR (pTLN8) and D50A BFR (pALN39) were confirmed by sequencing (MWG Biotech). A pET21a-derived construct (pTLN10) encoding the double variant H46A/D50A was obtained directly from Gen-Script (New Jersey, USA).

Protein Purification and the Removal of Nonheme Iron. Wild-type, H46A, D50A, and H46A/D50A BFRs were prepared as previously described.[11] Nonheme iron present on purification was removed by treatment with sodium dithionite and bipyridyl.[12] Heme contents of nonheme iron-free proteins, determined through the heme Soret absorbance intensity, using $\varepsilon_{418\ nm} = 107\ 000\ M^{-1}$ cm^{-1},[9] were found to be <1 for wild-type BFR, ~1.5 for H46A and D50A BFRs, and ~1.7 for H46A/D50A BFR. The concentration of wild-type and variant BFRs was determined using a per subunit $\varepsilon_{280\ nm}$ value of 33 000 $M^{-1}\ cm^{-1}$.[10]

Structural Methods. Nonheme iron-free (apo) BFR was crystallized by the hanging-drop vapor-diffusion method using a reagent composed of 1.8 M ammonium sulfate, 100 mM trisodium citrate pH 5. Crystal soaking experiments were performed by transferring apo-BFR crystals into a cryo-protectant solution composed of 1.65 M ammonium sulfate, 30% (v/v) glycerol, 100 mM MOPS pH 7 that was supplemented, as necessary, with 50 mM Fe(II)-$(NH_4)_2(SO_4)_2$, 50 mM Zn(II)SO_4, or a mixture of the two. All cryo-protectant solutions were prepared anaerobically and only exposed to oxygen for the duration of the crystal soaks. Apo data sets were collected at the European Synchrotron Radiation Facility (ESRF) beamline ID 23-1. All other data sets were obtained at the UK Synchrotron Radiation Source (SRS), station 10.1. X-ray data were processed using the CCP4 suite:[13] Indexing and integration used MOSFLM;[14] and data were scaled using SCALA.[15] A single monomer of 1BCF[7] (edited to remove side chains and energy-minimized to help remove potential model bias) was used in molecular replacement with MOLREP.[16] After density modification,[17] models were built and refined using COOT[18] and REF-MAC,[19] respectively. Tight geometry and 12-fold NCS-restraints

were applied throughout refinement and the same set of reflections (5%) were used in calculating R_{free} in all structures. For structures of crystals soaked in metal solutions, bound metals were identified by a combination of map-based techniques including the following: analysis of electron density maps in the refined structures; anomalous-difference Fourier analysis (using X-ray data collected at the relevant absorption edge); isomorphous-difference Fourier analysis; and, where metal-binding was detected, omit map analysis showing "unbiased" electron density for the bound ligands. Anomalous difference, isomorphous difference, and omit maps were calculated with FFT,[20] and 12-fold NCS-averaged versions of these maps were created using COOT. Metal-soak data sets were scaled to the apo data set using SCALEIT and isomorphous difference maps calculated using the difference in observed amplitudes between metal-soaked and apo data sets with phases derived from the apo-BFR structure; $2|F_o| - |F_c|$ omit maps used phases and $|F_c|$ values derived from models in which the bound metal ions were omitted. Structural figures were produced using PYMOL[21] and annotated with GIMP. Atomic coordinates have been deposited in the Protein Data Bank (PDB ID codes: 3E1J (apo), 3E1L (Phosphate-soak), 3E1O (Zn^{2+}-soak), 3E1P (Zn^{2+}/Fe^{2+}-soak), 3E1 M (Fe^{2+}-short soak), 3E1N (Fe^{2+}-long soak)).

Kinetic Methods. BFR catalyzed Fe^{2+} oxidation was measured at 340 nm using either a conventional UV−visible spectrophotometer (Perkin-Elmer λ35 or Hitachi U2900), for which Fe^{2+} additions were made using a microsyringe (Hamilton), or by using a stopped-flow apparatus (Applied Photophysics DX17MV). For multiple Fe^{2+} additions, oxidation was allowed to go to completion (constant $A_{340\ nm}$ value) before centrifuging samples (10 000 rpm, 5 min) to remove any Fe^{3+} not associated with the protein prior to subsequent additions. Rates of phase 3 Fe^{2+} oxidation were calculated from initial, linear increases in $A_{340\ nm}$ per unit time.[11]

Results and Discussion

The Metal-Free Ferroxidase Center is Preformed. BFR was crystallized in a metal-free (apo) form, and its structure solved. The overall subunit fold and arrangement of subunits was essentially identical to that previously reported.[7,22] Even in the absence of metal ions, the side chains of the ferroxidase center residues (Glu18, Glu51, His54, Glu94, Glu127, and His130) were clearly in position to bind metal ions; *i.e.*, the center is preformed, Figure 1A. Similar observations were made for *E. coli* FtnA (a bacterial nonheme-containing ferritin)[23] and for the R2 subunit of ribonucleotide reductase.[24] A ferroxidase center pore previously identified in *Desulfovibrio desulfuricans* BFR,[25] which provides access to the center from the outside, was also clearly present.

As a control for metal soaking experiments (see below), equivalent soaks of apo-BFR crystals in metal-free or sodium phosphate solutions were conducted. As expected these did not lead to the observation of metal ions. However, in the phosphate-soaked structure, some rearrangements of the side chains of His130 (see *Supporting Information* Figure S1) and the non-ferroxidase center residues Tyr25 and Glu47 were observed.

(12) Bauminger, E. R.; Harrison, P. M.; Hechel, D.; Nowik, I.; Treffry, A. *Biochim. Biophys. Acta* **1991**, *1118*, 48–58.
(13) Bailey, S. *Acta Crystallogr., D* **1994**, *50*, 760–763.
(14) Leslie, A. G. *Acta Crystallogr., D* **2006**, *62*, 48–57.
(15) Weiss, M. S. *J. Appl. Crystallogr.* **2001**, *34*, 130–135.
(16) Vagin, A.; Teplyakov, A. *J. Appl. Crystallogr.* **1997**, *30*, 1022–1025.
(17) Cowtan, K. *Jnt. CCP4/ESF-EAMCB Newslett. Prot. Crystallogr.* **1994**, *31*, 34–38.
(18) Emsley, P.; Cowtan, K. *Acta Crystallogr., D* **2004**, *60*, 2126–32.
(19) Murshudov, G. N.; Vagin, A. A.; Dodson, E. J. *Acta Crystallogr., D* **1997**, *53*, 240–55.

(20) Read, R. J.; Schierbeek, A. J. *J. Appl. Crystallogr.* **1988**, *21*, 490–495.
(21) DeLano, W. L. *The PyMOL Molecular Graphics System*; DeLano Scientific: San Carlos, USA, 2002.
(22) van Eerde, A.; Wolternik-van Loo, S.; van der Oost, J.; Dijkstra, B. W. *Acta Crystallogr., F* **2006**, *62*, 1061–1066.
(23) Stillman, T. J.; Hempstead, P. D.; Artymiuk, P. J.; Andrews, S. C.; Hudson, A. J.; Treffry, A.; Guest, J. R.; Harrison, P. M. *J. Mol. Biol.* **2001**, *307*, 587–603.
(24) Aberg, A.; Nordlund, P.; Eklund, H. *Nature (London)* **1993**, *361*, 276–278.
(25) Macedo, S.; Romao, C. V.; Mitchell, E.; Matias, P. M.; Liu, M. Y.; Xavier, A. V.; LeGall, J.; Teixeira, M.; Lindley, P.; Carrondo, M. A. *Nat. Struct. Biol.* **2003**, *10*, 285–290.
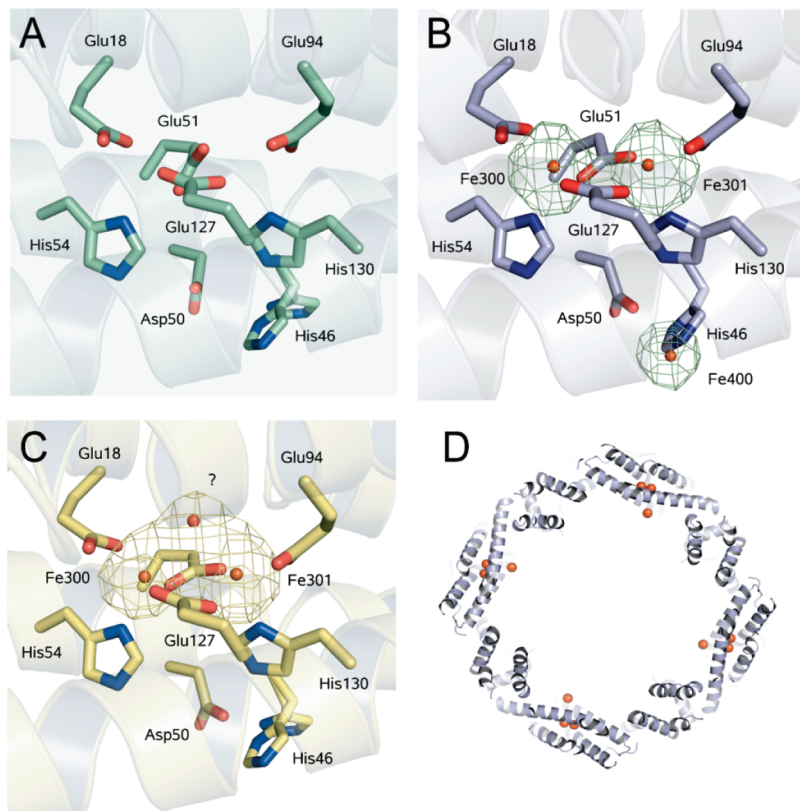
Figure 1. Crystal structures of BFR reveal three distinct catalytic states of the ferroxidase center. (A) Apo-ferroxidase center obtained after soaking an apo-BFR crystal aerobically (at pH 7) in a cryo-protectant solution devoid of iron. (B) Structure of a di-Fe^{2+} ferroxidase center intermediate with an additional iron site located on the inner face of each subunit obtained after a 2.5 min exposure to Fe^{2+}. The 12-fold NCS-averaged anomalous map constructed using diffraction data collected at the iron peak is shown as a green mesh (12 σ, 2.7 Å). (C) Structure of a probable μ-oxo bridged diferric intermediate, obtained in a 65 min aerobic soak using an anaerobically prepared solution of Fe^{2+}. A 12-fold NCS-averaged omit map (12 σ) is shown as a yellow mesh, with a question mark and red sphere denoting the additional bridging electron density. (D) A cross section of the biological unit (with metal ions shown as orange spheres) confirming that iron associated with Asp50 and His46 is located on the inside face of the BFR molecule and is associated with all 24 protein subunits. Further anomalous, omit, and isomorphous difference maps are available as Supporting Information for all metal-containing structures (see Figure S2). For clarity, crystallographic waters have been omitted from all panels.

This suggests that a degree of flexibility exists in the apo-form that could be important for binding of metals at the ferroxidase center. Data collection and refinement statistics for all structures reported here are given in Table 1.

Structure of the Di-Fe^{2+} Form of the Ferroxidase Center. Aerobic apo-BFR crystals were soaked in an Fe^{2+} solution and flash-frozen after 2.5 min. This resulted in binding of two iron atoms with full occupancy at each ferroxidase center. The di-iron site, in which the two irons are 3.71 Å apart, is roughly 2-fold rotationally symmetric, with each iron ligated by one histidine nitrogen and four carboxyl oxygens. Two of these oxygen ligands arise from a bidentate glutamate carboxyl (Glu18 in one site, and Glu94 in the second), and the others are supplied by Glu51 and Glu127 which straddle the two irons (Figure 1B and Figure S2A–C). The oxidation state could not be determined directly because X-ray crystallography is not able to distinguish between Fe^{2+} and Fe^{3+}, and X-ray fluorescence could not be used because the method is unable to distinguish between different iron atoms that are located in different environments (both within the protein and "free" in the soak solution). However, the two irons are very likely to be in the ferrous state. The center is structurally similar to those reported for Zn^{2+} (see below), a Mn^{2+}-occupied form,[7] and the di-Fe^{2+} form of *D. desulfuricans* BFR, which exhibited an almost identical inter-iron distance of 3.72 Å.[25] Furthermore, there is a lack of bridging electron density between the iron atoms, and all known stable

dinuclear iron centers containing two Fe^{3+} ions are bridged by an oxo/hydroxo species.[26]

Structure of the Bridged Di-Fe^{3+} Form of the Ferroxidase Center. Soaking of aerobic apo-BFR crystals in an Fe^{2+} solution for a longer period (65 min) also resulted in binding of two irons at the ferroxidase center at full occupancy. However, the electron density map also showed an additional structural feature bridging the two irons. The origin of the additional density cannot be established unequivocally due to the limits of resolution (2.8 Å); however, the omit density (Figure 1C and Figure S2D–E) is consistent with a small molecule such as H_2O, OH^-, O_2, H_2O_2, or O^{2-}. It is significant that the density is quite different from that observed for the "as-isolated" *D. desulfuricans* BFR di-Fe^{3+} center, which was concluded to arise from a heterogeneous mix of bridging species dominated by a bridging μ-peroxo intermediate.[25] The electron density observed here, is much smaller and symmetric, and most likely represents a form of the ferroxidase center dominated by a μ-oxo (or hydroxo) bridged di-Fe^{3+} form.

An inter-iron distance of 3.63 Å observed here is somewhat larger than that typically observed for bridged di-Fe^{3+} centers but is shorter than that reported for the di-Fe^{3+} form of *D. desulfuricans* BFR (3.71 Å), and we conclude that the oxidized form of the center is analogous to those previously observed in

(26) Kurtz, D. M. *J. Biol. Inorg. Chem.* **1997**, 2, 159–167.

Table 1. Data Collection and Refinement Statistics

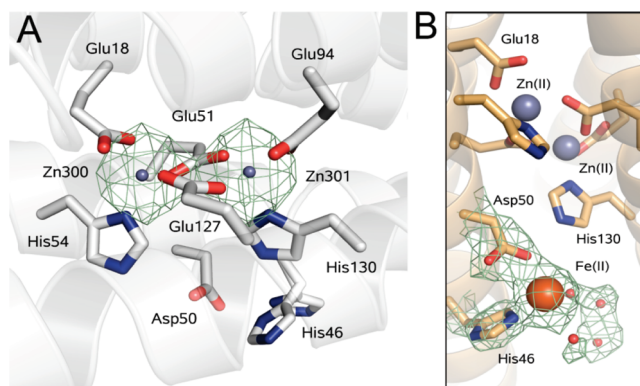|	Fe²⁺ 2.5 min	Apo	Zn²⁺	Zn²⁺/Fe²⁺	Fe²⁺ 65 min	Phosphate
	Data Collection Statistics					
space group	$P4_22_12$	$P4_22_12$	$P4_22_12$	$P4_22_12$	$P4_22_12$	$P4_22_12$
cell dimensions (Å)	$a = b = 207.97$,	$a = b = 208.22$,	$a = b = 208.87$,	$a = b = 207.40$,	$a = b = 207.74$,	$a = b = 208.08$,
	$c = 142.88$	$c = 142.46$	$c = 142.43$	$c = 142.45$	$c = 142.95$	$c = 143.11$
wavelength (Å)	1.740	1.072	1.282	1.737	1.739	1.739
resolution[a,b] (Å)	32−2.7	35−2.7	45−2.95	73.32−2.40	32.7−2.8	34.2−2.5
	[3.2−2.86]	[2.95−2.86]	[3.3−3.12]	[2.87−2.68]	[3.13−2.96]	[2.8−2.65]
	(2.85−2.7)	(2.85−2.7)	(3.11−2.95)	(2.53−2.4)	(2.95−2.8)	(2.64−2.5)
R_{sym}[a,b]	0.101 [0.123]	0.101 [0.176]	0.081 [0.135]	0.116 [0.274]	0.170 [0.393]	0.101 [0.221]
	(0.225)	(0.202)	(0.168)	(0.372)	(0.399)	(0.251)
$I/\sigma(I)$[a,b]	14.4 [13.4]	14.5 [7.3]	20.9 [11.3]	16.3 [7.8]	13.6 [5.1]	19.6 [7.4]
	(4.7)	(5.0)	(7.9)	(3.1)	(4.0)	(5.2)
completeness[a,b] (%)	85.3 [97.3]	98.8 [99.7]	89.2 [74.3]	97.0 [100.0]	98.1 [96.1]	96.4 [99.1]
	(46.8)	(93.7)	(56.9)	(83.3)	(91.9)	(80.7)
multiplicity[a,b]	7.4 [8.1]	6.5 [4.3]	9.1 [7.3]	12 [10.1]	11.0 [9.0]	13.9 [8.2]
	(4.3)	(3.1)	(6.5)	(3.9)	(8.8)	(5.7)
ano. completeness[a,b] (%)	84.1 [98.3]	96.3 [97.4]	88.2 [71.9]	95.1 [98.8]	96.0 [89.6]	95.6 [92.4]
	(42.7)	(83.1)	(53.4)	(75.8)	(87.0)	(77.9)
ano. multiplicity[a,b]	3.8 [4.2]	3.4 [2.2]	4.8 [3.9]	6.2 [5.1]	5.7 [4.8]	7.2 [4.2]
	(3.3)	(1.7)	(3.5)	(2.1)	(4.6)	(2.9)
	Refinement Statistics					
unique reflections	73 181	84 897	58 778	117 098	75 629	104 275
R_{work}, R_{free}[c]	0.241, 0.259	0.242, 0.263	0.229, 0.252	0.241, 0.260	0.250, 0.268	0.236, 0.248
free correlation coefficient	0.9279	0.9304	0.9370	0.9366	0.9251	0.9371
number of protein atoms	15 804	15 912	15 636	15 792	15 924	15 876
number of waters	246	399	214	863	246	496
rms bond (Å)	0.017	0.017	0.023	0.012	0.017	0.012
rms angle (deg)	1.760	1.817	1.941	1.439	1.856	1.368
	Isomorphous Scaling					
resolution[a] (Å)	30−3 (3.1−3.0)	30−3 (3.1−3.0)	30−3 (3.1−3.0)	−	30−3 (3.1−3.0)	−
R_{deriv}[a,d]	0.087 (0.117)	0.0 (0.0)	0.131 (0.159)	−	0.206 (0.261)	−

[a] Values in parentheses represent the highest resolution shell. [b] Values in square brackets denote the resolution bin at the detector edge. [c] Because of high NCS, the R_{Free} value reported here may well be undermined by correlations between reflections of the refinement and validation sets.[33] [d] Isomorphous scaling uses the Apo data set as reference.

the di-Fe^{3+} sites of other class II di-iron proteins such as ribonucleotide reductase and methane monooxygenase.[27,28]

Identification of a Novel Iron Site on the Inner Surface of BFR. The most striking feature of the structure of BFR containing Fe^{2+} was the presence of an additional iron site directly below the ferroxidase center on the inner face of the protein, associated with Asp50 and His46, Figure 1B. This iron is 9.2 Å from the nearest ferroxidase center iron and 10.2 Å from the second and clearly protrudes into the central cavity (Figure 1D). The occupancy of iron in the internal iron site was ~40%.

The internal surface iron site was not occupied in the structure of BFR containing Fe^{3+} ions at the ferroxidase center (Figure 1C). The observation of the three principal ferroxidase center intermediates over different periods of exposure to Fe^{2+} and O_2 demonstrates that mineralization can occur *in crystallo*. The iron status of the inner surface site is also consistent with this: the low occupancy of the internal-surface site in the di-Fe^{2+} structure and the complete absence of iron at the site in the di-Fe^{3+} structure indicate the incorporation of this iron into the growing iron mineral. We note that the iron mineral inside ferritins has so far eluded precise structural characterization due, presumably, to its heterogeneous composition and orientation relative to the protein coat.

Zn^{2+} has previously been shown to act as a potent inhibitor of BFR, through, it was proposed, its capacity to tightly bind

(27) Nordlund, P.; Sjoberg, B. M.; Eklund, H. *Nature (London)* **1990**, *345*, 593−598.
(28) Rosenzweig, A. C.; Frederick, C. A.; Lippard, S. J.; Nordlund, P. *Nature (London)* **1993**, *366*, 537−543.

Figure 2. Zinc inhibition of the ferroxidase center reveals fine structure of a novel internal iron site. (A) di-Zn^{2+}-form of the ferroxidase center obtained after soaking apo-BFR crystals for 5 min in Zn^{2+} at pH 7. The NCS-averaged anomalous map revealing zinc sites (green mesh) was constructed using X-ray data collected at the Zn^{2+}-peak wavelength (12 σ). (B) Structure of Zn^{2+}-inhibited BFR after exposure to Fe^{2+}. Apo-BFR crystals were soaked first in Zn^{2+} to inhibit iron oxidation at the ferrroxidase center and then again in a mixture of both Zn^{2+} and Fe^{2+} (for 5 min) before data collection. The resulting $2|F_o| - |F_c|$ electron density map (12 σ, teal mesh) reveals a full occupancy internal iron site with additional electron density resulting from the association of water molecules with this site.

at the ferroxidase center.[8,10,11] Crystals of apo-BFR were soaked in a Zn^{2+} solution, resulting in binding of two Zn^{2+} ions at the ferroxidase center, Figure 2A and Figure S2G−I, which has a structure very similar to the Mn^{2+} form of the center previously reported (with intermetal distances of 4.16 and 4.11 Å, respectively).[7] It is also apparent that Zn^{2+} does not bind at the Asp50/

His46 internal site or anywhere else within the protein, thus confirming the molecular basis of Zn^{2+} inhibition of 24-meric BFR.

Zn^{2+}-soaked apo-BFR crystals were subsequently soaked in a solution of Zn^{2+} and Fe^{2+}. In the resulting structure, Figure 2B, Zn^{2+} remained bound at the ferroxidase center, while the inner surface site was occupied by Fe^{2+} at 100% occupancy. As a consequence, the finer features of the electron density surrounding this iron were much clearer than those in the Fe^{2+}-only soak structure, revealing that the inner-surface iron is coordinated by only a single oxygen atom from Asp50, and the ε-Nitrogen of His46, with coordination completed by (up to) three partially ordered water molecules. These data surprisingly indicate that Fe^{2+} binds selectively (in competition with Zn^{2+}) at the inner surface site. The origin of this selectivity is currently unknown but could arise from the relative affinities of the site itself, or from access into the protein's central cavity. These structures also demonstrate that Fe^{2+} entry into the central cavity of BFR occurs independently of the ferroxidase center.

The Internal Surface Iron Site is Important for Mineralization. To investigate the functional importance of the inner surface iron site, the variants H46A, D50A, and H46A/D50A were generated. Each variant protein exhibited association state, stability, and UV−visible absorbance characteristics and ferroxidase center kinetic properties (see below) that were identical to those of the wild-type protein, indicating that they were properly folded. The kinetics of iron oxidation in the variants were studied and compared to the wild-type protein. $A_{340 \text{ nm}}$ changes following the addition of 400 Fe^{2+} ions per wild-type, H46A, D50A, and H46A/D50A BFR molecule were recorded, Figure 3A. For wild-type BFR, the addition of Fe^{2+} resulted in an initial, rapid increase in absorbance followed by a much slower increase. This biphasic kinetic behavior is well-documented:[8,9] the rapid phase corresponds to the oxidation of 2 Fe^{2+} ions at each ferroxidase center (termed phase 2), while the slower phase corresponds to the mineralization of iron within the BFR cavity (phase 3) and is only observed when all of the ferroxidase centers are filled. Phase 1, the very rapid binding of 2 Fe^{2+} ions at each ferroxidase center, is not directly measurable using this method but has been measured indirectly through its effect on the heme absorbance.[9] All three variants followed the same biphasic iron oxidation behavior as wild-type, but the rate of phase 3 mineralization was significantly impaired; the rate of iron oxidation for the variants (D50A: 4.4 ± 0.3 μM min^{-1}, H46A: 3.2 ± 0.2 μM min^{-1}, H46A/D50A: 3.1 ± 0.2 μM min^{-1}) was ~17−25% that of the wild-type (17.4 ± 0.5 μM min^{-1}), demonstrating that these residues are functionally important.

The initial rapid increase observed for each variant in Figure 3A indicated that the initial burst due to Fe^{2+} oxidation at the ferroxidase center (phase 2) was unaffected. Stopped-flow was used to analyze this phase in more detail. Titration of the single variant proteins with increasing levels of Fe^{2+} resulted in the observation of rapid phase 2 kinetics;[8,9] see Figure 3B and Figure S3 for data for H46A and D50A BFR, respectively. Plots of $\Delta A_{340 \text{ nm}}$ as a function of Fe^{2+}/BFR showed that they also exhibited unaffected saturation at ~2 Fe^{2+} ions per ferroxidase center (48 irons per 24mer), Figure 3C. Thus, in the variants, Fe^{2+}-binding and single turnover oxidation at the ferroxidase center occurred normally but iron mineralization within the cavity was significantly impaired, demonstrating that His46 and Asp50 play a significant role only in phase 3 of mineralization.
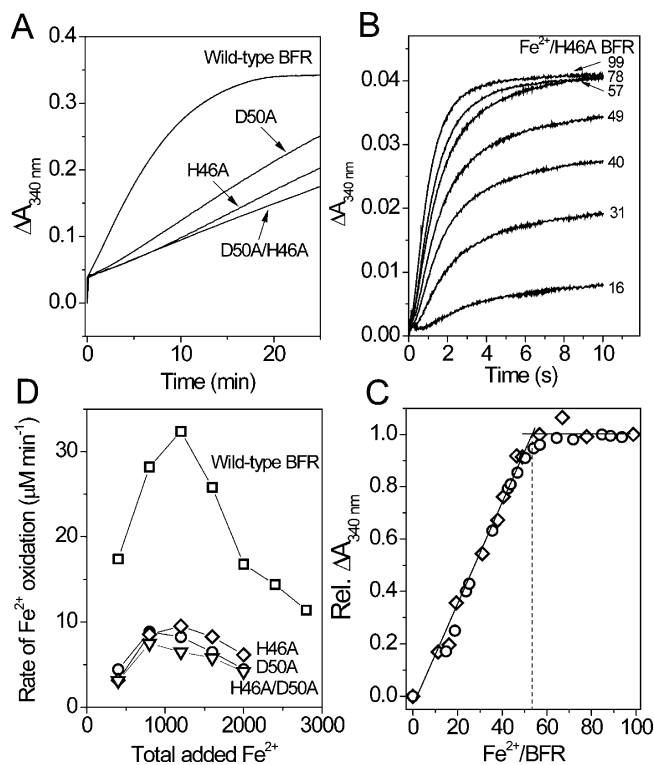
Figure 3. Kinetic analysis of inner surface site BFR variants. (A) $\Delta A_{340 \text{ nm}}$ as a function of time following additions of 400 Fe^{2+} ions per wild-type, H46A, D50A, and H46A/D50A BFR molecule. (B) $\Delta A_{340 \text{ nm}}$ measured by stopped-flow during the first 10 s following additions of 0−100 Fe^{2+} per H46A BFR. An equivalent plot for D50A is shown in the Supporting Information, Figure S3. (C) Plots of relative $\Delta A_{340 \text{ nm}}$ as a function of the Fe^{2+}/protein ratio for H46A ($\Diamond$) and D50A ($\bigcirc$) BFRs. Saturation of phase 2 is indicated by the intersection of initial and final linear regions of the plots. Data points are derived from (B) and from additional equivalent experiments. (D) Initial rates of Fe^{2+} oxidation following sequential additions of 400 Fe^{2+} to wild-type ($\square$), H46A ($\Diamond$), D50A ($\bigcirc$), and H46A/D50A ($\triangledown$) BFRs as a function of the total Fe^{2+} added. The proteins (0.5 μM) were in 0.1 M MES pH 6.5. Temperature was 25 °C, and path length 1 cm.

Rates of mineralization were subsequently measured for a series of additions of 400 Fe^{2+} ions per protein;[11] see Figure 3D. Clearly, iron mineralization in the variant proteins was significantly inhibited throughout core formation, regardless of the amount of iron that the protein has previously been exposed to. Thus, the cavity surface iron site is operational throughout the growth of the iron mineral and not only for the nucleation of new mineral particles.

Significance of the Inner Surface Site for Other Ferritins. While a carboxylate residue (Asp or Glu) at position 50 is very highly conserved, the presence of a histidine at position 46 is less so (see Supporting Information Figure S4). It is well conserved among BFRs from γ-proteobacteria and in cyanobacteria but is often replaced (in some cases by a glutamate, but in others by a nonligating residue) in BFRs from other bacteria. Thus, modified and/or alternative sites must exist in these BFRs. Interestingly, the inner surface site residues are conserved in many eukaryotic H-chain and L-chain ferritins, suggesting that iron sites similar to that described here may be involved, for example, in core nucleation in these proteins. Iron has not been identified bound to these residues in other ferritins but other metals have, for example, Zn^{2+} (in E27D/K86Q variant

of HuHF),[29] Mn^{2+} (in mitochondrial ferritin),[30] and Cd^{2+} (in mouse L-chain ferritin).[31] We also note that an iron site external to the ferroxidase center was previously identified in *E. coli* FtnA. The site (called Site C) is very different from that observed here in BFR, being ∼6 Å away from the ferroxidase center and close to, but not at, the protein surface.[23]

Mechanism of BFR Mineralization. The structural and kinetic data reported here provide significant new insight into the mechanism(s) of iron mineralization. The apo-form of the BFR ferroxidase center is primed ready to accept Fe^{2+} ions entering via the outer pore. In the presence of oxygen the Fe^{2+} ions are oxidized to Fe^{3+}, resulting in a μ-oxo (or hydroxo) bridged di-Fe^{3+} form of the center. Importantly, the data revealed no indication of instability of this form of the center and are entirely consistent with previous mechanistic studies[9,10] from which it was concluded that the BFR ferrroxidase center remains occupied throughout steady-state iron mineralization. Furthermore, there is no evidence for an unimpeded iron-transfer route from the ferroxidase center to the central cavity.

The data therefore support the notion that structural differences between the ferroxidase centers of BFR and H-chain ferritins result in large functional differences and that the center of BFR operates similarly to those of other class II di-iron proteins, *i.e.*, as a true catalytic center, rather than as a pore for iron transfer into the cavity. In this way, BFR represents a significant evolutionary connection between di-iron enzymes (in which iron is a cofactor) and H-chain ferritins (in which iron is the substrate).[32]

Fe^{2+}, present in excess of that required to saturate the ferroxidase center sites, enters the BFR central cavity. Here, we have identified an initial binding site, formed by Asp50 and His46, for Fe^{2+} in the cavity and established that it is functionally important: variants lacking either or both amino acid residues are specifically impeded in phase 3 mineralization. That mineralization was not completely blocked when both inner surface site residues were substituted indicates that, although of principal importance, the site described here is not the only one at which Fe^{2+} ions can bind on the inner surface; such a site(s) may not be amenable to detection by crystallographic methods. The inner surface site appears to be functionally connected to the ferroxidase center; the occupancy of the site was found to be directly correlated with the status of the ferroxidase center, and 100% occupancy was only achieved by inhibiting the ferroxidase center activity with Zn^{2+} ions.

What is the functional connection between the ferroxidase center and the inner surface site? Although the inner surface site may be important for core nucleation, we favor a model, based on, and consistent with, all available data, in which the major role of the inner surface site, located ∼10 Å directly below the ferroxidase center, is to facilitate electron transfer from Fe^{2+} ions in the central cavity to the ferroxidase center. Such a model accounts for how the ferroxidase center, which functions as a di-iron cofactor, and which is essential throughout the miner-
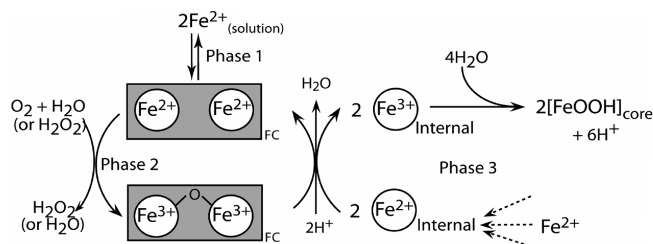
Figure 4. Proposed mechanism of iron mineralization in BFR. Schematic diagram emphasizing the role of the ferroxidase center as a true catalytic site that cycles between di-Fe^{2+} and μ-oxo bridged di-Fe^{3+} forms to mediate electron transfer from Fe^{2+} in the protein core to a suitable electron acceptor in the ferroxidase center pocket, such as O_2 or H_2O_2.

alization process,[1,11] acts to drive Fe^{2+} oxidation in the cavity. In a continual catalytic cycle, the di-Fe^{3+} center is rereduced by electrons derived from the oxidation of Fe^{2+} ions in the cavity, and the di-Fe^{2+} form is subsequently oxidized by reaction with oxygen (or hydrogen peroxide). Consistent with this, disruption of the inner surface site (by mutagenesis) did not affect the activity of the ferroxidase center (i.e., phase 2 oxidation was unaffected) but, we propose, instead inhibited the route for ferroxidase center reduction and therefore phase 3 of the mineralization process. A schematic view of the proposed mechanism is shown in Figure 4. As two electrons are required to reduce the bridged di-Fe^{3+} ferroxidase center, the observation of a single inner surface Fe^{2+} site raises questions about the precise details of the mechanism by which the ferroxidase center becomes reduced. One possibility is that electrons may be derived from more than one inner surface Fe^{2+} site, but alternatives exist and await further detailed investigation.

In summary, the data presented here, together with previous mechanistic studies, provide a detailed structural and mechanistic picture of protein coat-directed biomineralization. While it is clear that a catalytic center for Fe^{2+} oxidation, routes for Fe^{2+} access into the central cavity, and the ability to efficiently initiate core mineralization are common requirements for all ferritins, it is also clear that, despite broad conservation of ferritin structure and physiological function, significant variations exist in, for example, the structure of the catalytic ferroxidase center, the nature of the channels connecting the cavity with the outside, and the ligands to the internal surface iron site(s). The result of this is that the mechanism of mineralization also varies within ferritin proteins.

Supporting Information Available: Structure of the metal free ferroxidase center of *E. coli* BFR at pH 7 following soaking in sodium phosphate pH 7 (Figure S1); Structures of the *E. coli* BFR ferroxidase center in di-Fe^{2+}, bridged di-Fe^{3+}, and di-Zn^{2+} forms (Figure S2); Absorption changes at 340 nm in the first 10 s following additions of Fe^{2+} to D50A BFR (Figure S3); Partial amino acid residue sequence alignment of ferritins (Figure S4). This material is available free of charge via the Internet at http://pubs.acs.org.

(29) Toussaint, L.; Bertrand, L.; Hue, L.; Crichton, R. R.; Declercq, J. P. *J. Mol. Biol.* **2007**, *365*, 440–452.
(30) d'Estaintot, B. L.; Paolo, S.; Granier, T.; Gallois, B.; Chevalier, J. M.; Precigoux, G.; Levi, S.; Arosio, P. *J. Mol. Biol.* **2004**, *340*, 277–293.
(31) Granier, T.; d'Estaintot, B. L.; Gallois, B.; Chevalier, J. M.; Precigoux, G.; Santambrogio, P.; Arosio, P. *J. Biol. Inorg. Chem.* **2003**, *8*, 105–111.
(32) Liu, X. F.; Theil, E. C. *Proc. Natl. Acad. Sci. U.S.A.* **2004**, *101*, 8557–8562.
(33) Fabiola, F.; Korostelev, A.; Chapman, M. S. *Acta Crystallogr., D* **2006**, *62*, 227–238.

JA8093444